Electrokinetic Injection Techniques in Microfluidic Chips

ARTICLE *in* ANALYTICAL CHEMISTRY · NOVEMBER 2002

Impact Factor: 5.64 · DOI: 10.1021/ac025821w · Source: PubMed

Anal. Chem. **2002,** *74,* 5084−5091

Electrokinetic Injection Techniques in Microfluidic Chips

L.-M. Fu, R.-J. Yang,* G.-B. Lee, and H.-H. Liu

Department of Engineering Science, National Cheng Kung University, Tainan, 70101 Taiwan

The separation efficiency of a microfluidic chip is influenced to a significant degree by the flow field conditions within the injection microchannel. Therefore, an understanding of the physics of the flow within this channel is beneficial in the design and operation of such a system. The configuration of an injection system is determined by the volume of the sample plug that is to be delivered to the separation process. Accordingly, this paper addresses the design and testing of injection systems with a variety of configurations, including a simple cross, a double-T, and a triple-T configuration. This paper also presents the design of a unique multi-T injection configuration. Each injection system cycles through a predetermined series of steps, in which the electric field magnitude and distribution within the various channels is strictly manipulated, to effectuate a virtual valve. The unique multi-T configuration injection system presented within this paper has the ability to simulate the functions of the cross, double-T, and triple-T systems through appropriate manipulations of the electric field within its various channels. In other words, the proposed design successfully combines several conventional injection systems within a single microfluidic chip.

Recently, microfluidic devices have been used successfully in micro total analysis system (μ-TAS) applications such as capillary electrophoresis (CE)[1−3] and DNA separation.[4,5] The fundamental feature common to all of these techniques is that it is possible to control the movement of differently charged particles when they are prompted into motion due to the application of an external electric field. This induced flow motion is commonly referred to as electroosmotic flow.[6,7] The injection and separation microchannels used within the electrophoresis process are usually designed within a compact area of a microfabricated chip. Handling of the fluid is generally carried out by a series of electrokinetic manipulations, which can be used to deliver the sample to locations where it may be chemically modified,[8] diluted or mixed with other substances,[9,10] detected, or perhaps subjected to further analysis by coupling the microfluidic chip with other analytical techniques such as mass sepectroscopy.[11,12]

The injection system on a microfluidic chip is one of the key elements in the sample handling process, and its characteristics determine the quality of the separation achieved. Therefore, a thorough understanding of the mechanisms governing electrokinetic manipulations, particularly those associated with discrete injections, is important in the optimization of microfluidic chip design. A review of the published literature in this field reveals the existence of many discussions relating to cross-injection systems on microfluidic chips.[13−18] Generally, these injection systems are only capable of delivering a fixed-volume sample plug into the separation channel. However, some detection cases may require the delivery of larger-volume sample plugs to the separation process. For example, larger-volume sample plugs are required in multifraction collection devices.[19] In such cases, fixed-volume injection systems are clearly inappropriate. This limitation may be overcome by implementing injection systems with different configurations. The current paper considers the double-T-form configuration and the triple-T-form arrangement and also proposes a unique multi-T-form injection system. The various configurations all provide the ability to increase the volume of the sample plug delivered into the separation channel.

The primary goal of this study is to research the optimum design of injection channels and to investigate the ideal operating

* Corresponding author. E-mail: rjyang@mail.ncku.edu.tw. Tel: +886-6-275-7575 Ext. 63343. Fax: +886-6-276−6549.

(1) Culbertson, C.; Ramsey, R.; Ramsey, J. M. *Anal. Chem.* **2000**, *72*, 2285−2291.
(2) Hunter, R. J. *Zeta Potential in Colloid Science: Principles and Applications*; Academic Press: New York, 1981.
(3) Russel, W. B.; Saville, D. A.; Schowalter, W. R. *Colloidal Dispersions*; Cambridge University Press: New York, 1989.
(4) Effenhauser, C. S.; Paulus, A.; Manz, A.; Widmer, H. M. *Anal. Chem.* **1994**, *66*, 2949−2953.
(5) Woolley, A. T.; Mathies, R. A. *Anal. Chem.* **1995**, *67*, 3676−3680.
(6) Yang, R.-J.; Fu, L. -M.; Lin, Y.-C. *J. Colloid Interface Sci.* **2001**, *239*, 98−105.
(7) Yang, R.-J.; Fu, L.-M.; Hwang, C.-C. *J. Colloid Interface Sci.* **2001**, *244*, 173−179.
(8) Jacobson, S, C.; Hergenroder, R.; Moore, A. W.; Ramsey, J. M. *Anal. Chem.* **1994**, *66*, 4127−4132.
(9) Bianchi, F.; Ferrigno, R.; Girault, H. H. *Anal. Chem.* **2000**, *72*, 1987−1993.
(10) Culbertson, C. T.; Ramsey, R. S.; Ramsey, J. M. *Anal. Chem.* **2000**, *72*, 2285−2291.
(11) Xue. Q.; Foret, F.; Dunayevskiy, Y. M.; McGruer, N. E.; Karger, B. L. *Anal. Chem.* **1997**, *69*, 426−430.
(12) Ramsey, R. S.; Ramsey, J. M. *Anal. Chem.* **1997**, *69*, 1174−1178.
(13) Jacobson, S. C.; Ramsey, J. M. *Anal. Chem.* **1997**, *69*, 3212−3217.
(14) Jacobson, S, C.; Culbertson, C. T.; Daler, J. E.; Ramsey, J. M. *Anal. Chem.* **1998**, *70*, 3476−3480.
(15) Jacobson, S. C.; Ermakov, S. V.; Ramsey, J. M. *Anal. Chem.* **1999**, *71*, 3273−3276.
(16) Ermakov, S. V.; Jacobson, S. C.; Ramsey, J. M. *Anal. Chem.* **2000**, *72*, 3512−3517.
(17) Patankar, N. A.; Hu, H. H. *Anal. Chem.* **1998**, *70*, 1870−1881
(18) Alarie, J. P.; Jacobson, S. C.; Ramsey, J. M. *Eletrophoresis* **2001**, *22*, 312−317.
(19) Khandurina, J.; Chovan, T.; Guttman, A. *Anal. Chem.* **2002**, *74*, 1737−1740.

10.1021/ac025821w CCC: $22.00
Published on Web 08/27/2002

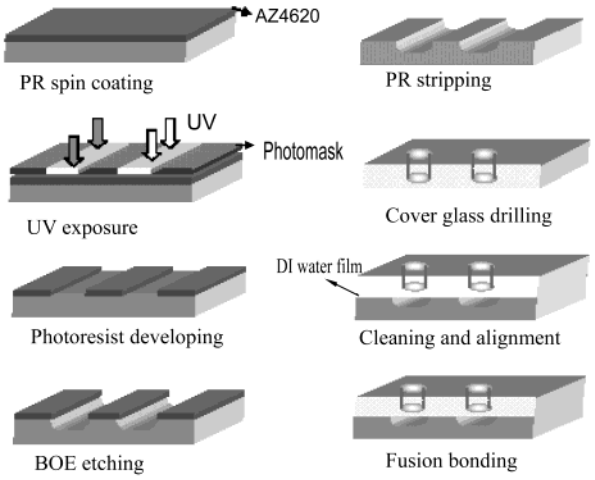

Figure 1. Fabrication of glass-based microchannel.

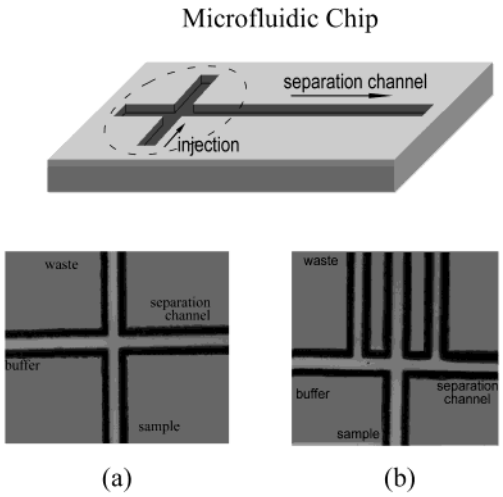

Figure 2. Photograph of two injection systems (a) cross and (b) multi-T.

conditions. Through model simulations, it is possible to determine the parameters that are key to controlling the shape of the injection sample plug. The effects of operating parameters such as the electric potential and the flow field are studied, and the theoretical results are used to fabricate and test several injection microfluidic chips, including one chip that contains a unique multifunction injection system. The resulting designs are investigated both theoretically and experimentally.

EXPERIMENTAL PROCEDURE

Microfabrication. The present study used commercially available microscope glass slides of dimensions 76 × 26 × 1 mm, supplied by Marienfeld. Prior to microfabrication of the glass chips, the slides were first annealed at 400 °C for 4 h in order to relieve their internal residual stress. Figure 1 illustrates the fabrication process[20−22] used in this study. Initially, the glass slide was cleaned with a piranha solution (H_2SO_4(%)/H_2O_2(%) = 3:1) for 10 min. It was then rinsed in DI water and blown dry with nitrogen gas. To ensure the complete removal of residual water molecules, a dehydration process was carried out by baking the slides on a hot plate for 3 min at a temperature of 100 °C.

Following the dehydration process, the slide was coated with the AZ4620 positive photoresist (PR) using a spin coater and then baked at 100 °C for a further 3 min. After soft baking, the thickness of the PR layer was measured to be ∼3 μm. The UV lithography was processed using a mask aligner (OAI Corp.) with an exposure dose of 180 mJ·cm^{-2}. Development process of the PR layer was accomplished by immersing the exposed substrate into a developer solution (AZ400k:DI water = 1:3) for 70 s. The resulting photoresist patterns were then hard-baked at 150 °C for 10 min. Since the baked PR layer is able to accommodate BOE (6:1) etching for as long as 40 min, there was no requirement for polysilicon, nitride, or gold layers during the masking process. BOE etching of the slides was performed in an ultrasonic bath. The slides were then rinsed with 1 M HCl solution.

Through holes with a diameter of 1.5 mm were drilled for sample inlets and outlets on another cover plate. The base and cover plates were fusion-bonded in a furnace at 580 °C for 20 min. The etching depth is 39.95 μm, and the surface roughness could be as small of 30 Å. Alternatively, a low-temperature glass bonding process using diluted HF (1%) has also been developed for sealing of microfluidic structures. Figure 2 shows the two geometries of the injection microchannel on glass substrates after photolithography process.

Detection. Performance of the microchips was monitored by a laser-induced fluorescence (LIF) method using a charge-coupled device (CCD; model TE/CCD512TKM) for imaging. For CCD imaging, an argon laser beam (514.5 nm, 100mW) was expanded to ∼5-mm diameter at the surface of the microchip using a lens. The fluorescence signal was collected using an optical microscopy (model TE300 Nikon, Melville, NY), filtered spectrally (550 nm, cut-on), and measured by CCD. Rhodamine B (9.1 μm, Aldrich, Milwaukee, WI) was used as the test sample. The buffer used for experiments was 10 mM sodium borate (pH 9.2, Aldrich).

FORMULATION

In electroosmotic flow, the fluid motion is driven principally by an applied electric potential rather than by a pressure force. Pressure-driven flow requires the use of a micropump, and so the production cost of the separation system is expensive and the operation process is difficult to control. A more convenient alterative is to drive fluid motion by applying an electric field to the net fluid charge in order to produce a body force.

Most studies regarding eletroosmotic flows[23−26] assumed the velocity profile to be fully developed in the microchannels and considered the charge density to conform to the Boltzmann equilibrium distribution. However, since electroosmotic flow requires an entance region where the velocity profile is not fully developed and the change density is not in Boltzmann equilibrium, these assumptions are not actually true. To include this entrance

(20) Lin, Y. H.; Lee, G. B.; Li, C. W.; Huang, G. R.; Chen, S. H. *J. Chromatogr., A* **2001**, *937*, 115−125.
(21) Lee, G. B.; Hwei, B. H.; Huang, G. R. *J. Micromech. Microeng.* **2001**, *11*, 654−661.
(22) Lin, C. H.; Lee, G. B.; Lin, Y. H.; Chang, G. L. *J. Micromech. Microeng.* **2001**, *11*, 726−732.
(23) Arulanandam, S.; Li, D. *Colloids Surf., A* **2000**, *161*, 89−102.
(24) Qu, W.; Li, D. *J. Colloid Interface Sci.* **2000**, *224*, 397−407
(25) Griffiths, S.; Nilson R. H. *Anal. Chem.* **2001**, *73*, 272−278.
(26) Dutta, P.; Beskok, A. *Anal. Chem.* **2001**, *73*, 1979−1986.

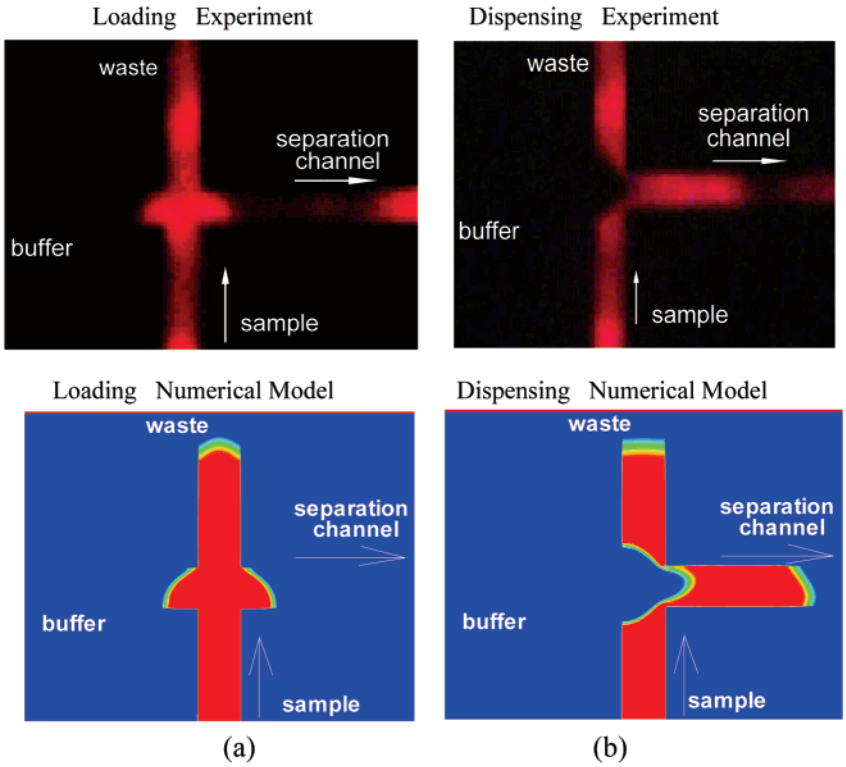

Figure 3. Comparison of the (a) loading and (b) dispensing steps of sample distributions between the numerical simulation and experimental results.

effect, the current authors have developed physical models[6,7,27] based on (a) the Poisson equation for the electric potential and ζ-potential, (b) the Nernst−Planck equations for ionic concentration, and (c) the full Navier−Stokes equations modified to include the effects of the body force due to the electric and the charge density. Finally, the concentration equation for a sample plug is also computed to simulate its distribution. The computational domain is considered from entry region to fully developed region. Since the flow rate is very small, yielding to very short entrance length. The separation is performed after the entrance region. Therefore, the entrance effect has nearly no effect on the results of separation. By introducing the reference quantities, L_{ref}, U_{ref}, p_{ref}, and ρ_{ref}, and defining $\bar{\rho}_e = \rho_e/n_0ze = (n^+ - n^-)/n_0$, $\bar{\psi} = ze\psi/k_bT$, $\bar{t} = tU_{ref}/L_{ref}$, $\bar{u} = u/U_{ref}$, $\bar{v} = v/U_{ref}$, $\bar{x} = x/L_{ref}$, $\bar{y} = y/L_{ref}$, $\bar{p} = (p - p_{ref})/(\rho U_{ref}^2)$, $\bar{\rho} = \rho_f/\rho_{ref}$, $\bar{n^+} = (n^+ - n_0)/n_0$, $\bar{n^-} = (n^- - n_0)/n_0$, the dimensionless form of governing equations after dropping the head symbols can be written as

$$\nabla^2\psi = -(\kappa^2/2)\rho_e \tag{1}$$

$$\frac{\partial n_i}{\partial t} + \vec{u}\nabla n_i = \frac{1}{ScRe}\nabla^2 n_i + \frac{1}{ScRe}[\nabla(n_i\nabla\psi)] \tag{2}$$

$$\nabla\cdot\vec{u} = 0 \tag{3}$$

$$\frac{\partial\vec{u}}{\partial t} + \vec{u}\cdot\nabla\vec{u} = -\nabla p + \frac{1}{Re}\nabla^2\vec{u} - G_x\rho_e\nabla\psi \tag{4}$$

$$\frac{\partial C}{\partial t} + \vec{u}\cdot\nabla C = \frac{1}{ScRe}\nabla^2 C \tag{5}$$

where $\kappa = W \times K$, $K = (2n_0z^2e^2/\epsilon\epsilon_0k_bT)^{1/2}$ is the Debye−Huckel parameter, "$1/K$" is the characteristic thickness of the charge density, $\rho_e = (n^+ - n^-)ze$ is the charge density, ϵ is the dielectric constant of the medium, ϵ_0 is the permittivity of a vacuum, n^+ and n^- are the concentrations of the positive and negative ions, n_0 is the bulk concentration of ions, k_b is Boltzmann's constant, T is the absolute temperature, $L_{ref} = W$, W is the channel height, $U_{ref} = \psi_{inlet}\epsilon\epsilon_0\zeta/\mu L$, ψ_{inlet} is the activated potential at inlet, $Re = \rho_fU_{ref}L_{ref}/\mu = \rho_f(\psi_{inlet}\epsilon\epsilon_0\zeta/\mu L)(L_{ref}/\mu)$ is the Reynolds number, $Sc = \mu/\rho_fD_i$ is the Schmidt number, μ is the liquid viscosity, ρ_f is the fluid density, ζ is the surface zeta potential, p is the pressure, $Gx = 2n_0k_bT\rho_fW^2/\mu Re^2$ is the ratio of the EDL energy to the mechanical kinetic energy, and C is the sample concentration. In this equation at hand, Sc is of the order of 10^5 and Re is of the order of 1. Therefore, the diffusion term is very small in comparison to the convection term. However, since diffusion is one of the primary mechanisms for sample dispersion, the term is retained in the numerical simulation. Since the concentration of the sample is carried passively by the flow field, eq 5 can be solved separately once the flow field is known.

Boundary Conditions and Numerical Method. In most of the electrophoresis experiments, the microchannel is filled with an aqueous electrolyte solution. The sample is injected into the channel, and then an electric potential is activated in order to carry out sample separation. Consequently, the initial conditions are assumed to be that the velocity is static everywhere and that the ζ-potential of the wall is given by $\psi|_{wall} = \varsigma$. Furthermore, the ionic concentration and potential are assumed to conform to Boltzmann

(27) Fu, L.-M.; Yang, R.-J.; Lee, G.-B. *Electrophoresis* **2002**, *23*, 602−612.
(28) Chorin, A. J. *J. Comput. Phys.* **1967**, *2*, 12−26.
(29) Yang, R.-J.; Jeng, Y.-R.; Fu, L.-M. *Comput. Fluid Dyn. J.* **1999**, *7*, 397−404.

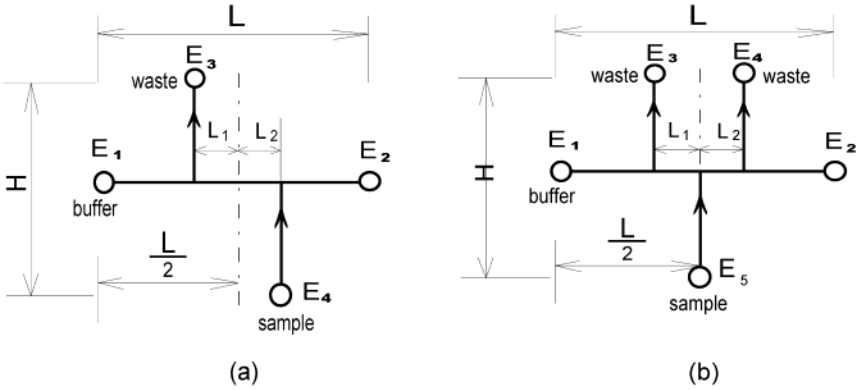

Figure 4. Schematics of (a) double-T-form and (b) triple-T-form injection systems.

equilibrium distribution initially. The detailed expressions of the initial conditions, the boundary conditions, and numerical method are given in the Supporting Information.

RESULTS AND DISCUSSION

The previous section presented equations and boundary conditions for the general case. In the current study, it is assumed that the microchannel is made of silica glass; the buffer fluid is sodium borate. The physical and electric properties of the liquid are as follows: dielectric constant $\epsilon = 80$, zeta potential of the channel wall $\zeta = -75$ mV, electrokinetic diameter $\kappa = 32$, viscosity of the fluid $\mu = 10^{-3}$ N·s/m^2, Schmidt number of the charge density $Sc = 10^5$, and diffusion coefficient of the sample (hemoglobin) $D = 6.9 \times 10^{-11}$ m^2/s.

Traditionally, the design of the injection channel has always been in the form of a cross. A limitation of this configuration is that it is only capable of providing discrete, fixed-volume samples. However, as stated previously, some applications require the delivery of different sample volumes to the detection and separation processes. Therefore, the present study replaces the traditional cross-channel configuration with double-T, triple-T, and multi-T injection channels and determines the optimum design and operating conditions for each configuration. Through careful control of the electric potential within the injection channels, these configurations provide the ability to increase the amount of sample delivered.

Cross-Injection System. In the injection technology of separation microchannels, the cross microchannel has been often used. The operation steps of the sample injection include loading and dispensing steps. Injection of the sample involves loading and dispensing steps. The controlling electric field in the loading and the dispensing step is established according to Kirchhoff's law,[15,16] which is defined as

$$\sum_i E_x/E_{\max} = \sum_j E_y/E_{\max} \tag{6}$$

where E_x and E_y are the electric field strengths along x and y directions, respectively, and $E_{\max}$ is the maximum field value. Note that Kirchhoff's law estimates the overall electric field. To identify the individual components of the electric potential (for example, ϕ_1, ϕ_2, ϕ_3, and ϕ_4 in the loading step, where $E = -\nabla\phi$), it is first necessary to establish a referenced electric potential. In the current study, the equivalent electric potential gradient was used to prevent flow along the x direction during the loading step and to prevent flow along the y direction in the dispensing step, i.e., by controlling $\partial\phi/\partial x$ and $\partial\phi/\partial y$, respectively. The mathematical model for the injection process can be written as

loading step

$\phi_{L,4} = \phi_{\max}$, $\phi_{L,3} = 0$

already known (established according to need)

$$\phi_{L,1} = \phi_{L,2} = ((\phi_{L,3} + \phi_{L,4})/2H)L \tag{7}$$

dispensing step

$\phi_{D,1} = \phi_{\max}$, $\phi_{D,2} = 0$

already known (established according to need)

$$\phi_{D,3} = \phi_{D,4} = ((\phi_{D,1} + \phi_{D,2})/2L)H \tag{8}$$

Equations 7 and 8 can quickly and accurately calculate each component of the electric potential required in the loading and dispensing steps for each component. This method reduces the trial and error approach that is necessary to establish the electric field in operating systems. The electric potential contour, velocity vector, and streamline of the loading and dispensing steps were presented in Figure S1 (see Supporting Information).

Simulation concentration distributions of sample are compared in Figure 3 with experimentally obtained CCD images. This figure shows two pairs of pictures corresponding to different steps. In each pair, the top picture shows an experimental image and the bottom one shows the simulated image. The results show good qualitative agreement. The agreement provides confidence in the ability of the proposed numerical simulation to predict the behavior of electrokinetic injections. Consequently, the paper now focuses upon the design of some new injection systems with enhanced injection characteristics.

T-Form Injection Systems. In the cross-channel system, the volume of the sample plug is determined by the geometry of the cross-sectional area of the injection channel. An implication of this is that the sample volume delivered by such a system is always constant. Therefore, this arrangement is clearly unsuitable for applications that require the supply of larger sample plugs to the separation process. A more appropriate solution is to replace the cross-channel arrangement with double-T-form or triple-T-form injection systems such as those shown schematically in Figure 4.

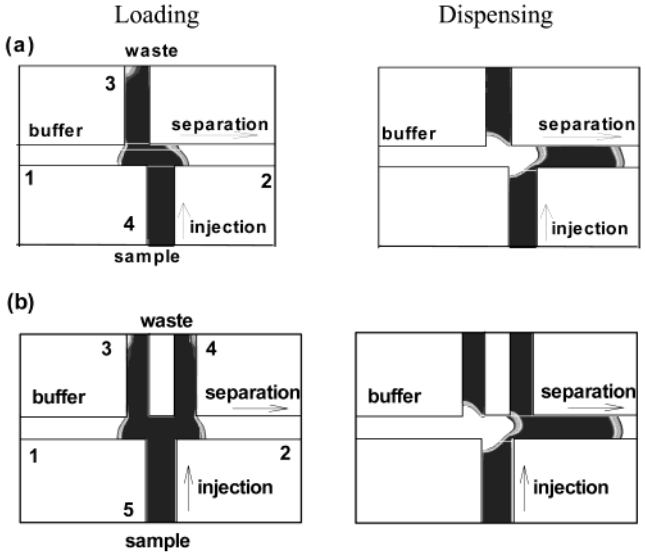

Figure 5. Injection of sample distributions of the (a) double-T-form (b) triple-T-form injection system.

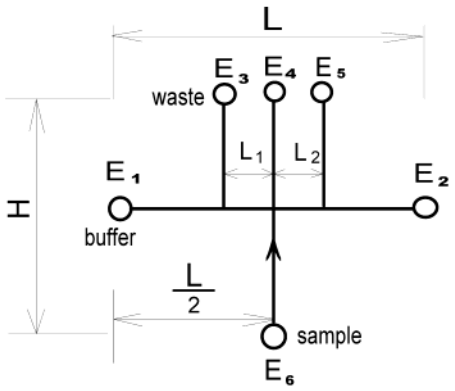

Figure 6. Schematics of multi-T-form injection system.

Table 1

	electric potential strengths (kV)					
	ϕ_1	ϕ_2	ϕ_3	ϕ_4	ϕ_5	ϕ_6
cross model loading	0.6	0.6	0.6	0	0.6	1.2
double-T model loading	0.5	0.42	0.5	0	0	1.2
triple-T model loading	0.42	0.42	0	0	0	1.2
dispensing	1.4	0	0.89	0.75	0.61	0.75
channel width (μm)	100	100	80	100	80	100

The mechanism used to control the electric potential within the microchannels is very important in both cases. They must satisfy Kirchhoff's law and conform to the mathematical models listed in appendixes A1 and A2 (Supporting Information). From appendixes A1 and A2, those equations can establish the electric potential of each component of the double-T-form and triple-T-form injection systems. The detailed electric potential contours and velocity streamlines of the loading and dispensing steps of the two injection systems were given in Figures S2 and S3 (Supporting Information).

Figure 5a presents the distribution of the sample injection using the double-T-form injection system. It can be seen that when the electric field is activated during the loading step, the sample flows from the injection channel 4 to the waste channel 3. Meanwhile, the potential distribution within the buffer channel 1 and the separation channel 2 is strictly controlled at a constant value in order to prevent sample leakage (Figures 5a, loading step). Once the sample has filled the intersection in the double-T area, the sample plug is led into separation channel 2 by establishing a linear potential distribution within the horizontal channels. During this dispensing step, the sample fluid in channels 3 and 4 is kept motionless (Figure 5a, dispensing step). After completion of the dispensing step, the electric field reverts back to its loading step conditions, and the system returns to its original state. It is clear that the volume of sample plug in the separation channel is larger in the double-T-form injection system than in the cross-injection system. If the detection application requires an even larger sample plug for separation, the triple-T-form injection system is an appropriate solution. The manipulation model of the triple-T-form injection system is similar to that of the double-T-form injection case. Figure 5b presents the distribution of a continuous sample injection for the triple-T-form injection system. Observation of this figure indicates that the volume of the sample plug in the separation channel is significantly greater than in the previous two cases.

A Unique Multi-T-Form Injection System. The previous discussions have introduced three types of injection system, namely, the traditional cross form, the double-T form, and the triple-T form. The cross-form and the double-T-form systems are independent in the sense that a single microfluidic chip only supports one form of injection system—i.e., the cross form or the double-T form. The triple-T form, however, may be used to simulate the function of the double-T form by controlling the voltage application sequence in a manner similar to the multi-T form to be described later. As has been shown, the sample plug volume delivered to the separation process is determined by the nature of the injection system implemented on any particular microfluidic chip. Furthermore, the plug size is constant for each type of injection system. Therefore, it will be appreciated that these injection systems are somewhat inflexible. This paper now presents the design of a unique multi-T-form injection system that combines the functions of cross, double-T-form, and triple-T-form injection systems on a single microfluidic chip. Figure 6 presents a schematic view of the proposed multi-T-form injection system. In this figure, the width of waste channels 3 and 5 is 0.8 times that of loading channel 6, which ensures that the time required to load the three waste channels (i.e. 3−5) is consistent. Control of the electric potential distribution through the loading and dispensing steps is similar to that described previously. By appropriate control of the electric potential, the proposed multi-T-form injection system is capable of replicating the operation of the three injection systems introduced above.

Case I: Cross-Injection System Model. In this mode, the multi-T-form injection system imitates the operation of the cross-injection system. However, the control of the electric potential that is necessary to achieve this is more complex than in the case of the original system and therefore it is necessary to specify the mathematical description of the electric potential that should be

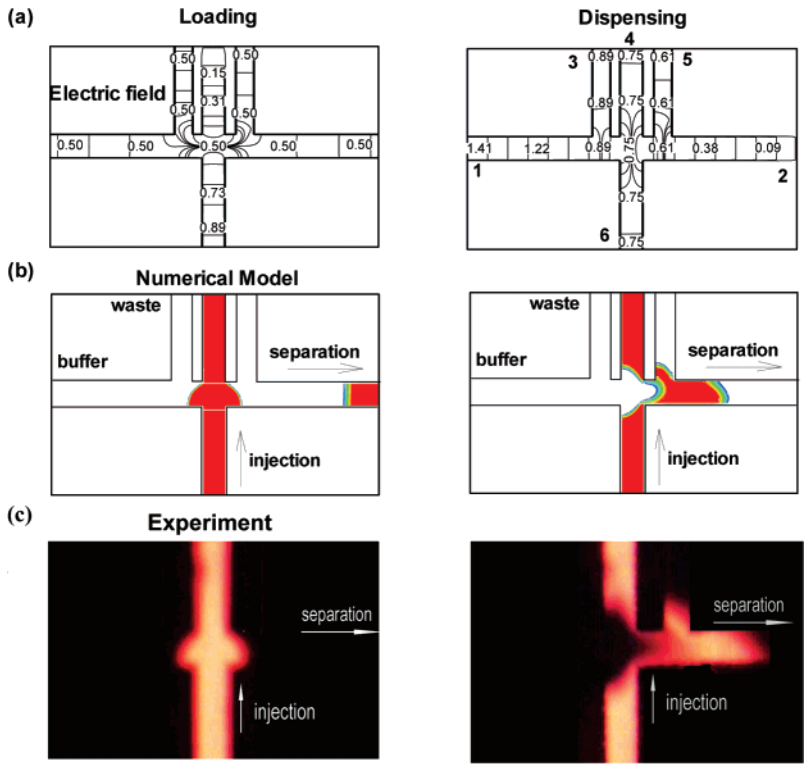

Figure 7. Cross-injection model of the multi-T-form injection system.

used. The mathematical model can be expressed as follows:

loading step

$\phi_{L,6} = \phi_{max}$, $\phi_{L,4} = 0$

already known (established according to need)

$$\phi_{L,1} = \phi_{L,3} = \left(\frac{\phi_{L,4} + \phi_{L,6}}{2H}\right)\left(1 + \frac{L_1}{L}\right)L \quad (9)$$

$$\phi_{L,2} = \phi_{L,5} = \left(\frac{\phi_{L,4} + \phi_{L,6}}{2H}\right)\left(1 - \frac{L_2}{L}\right)L \quad (10)$$

dispensing step

$\phi_{D,1} = \phi_{max}$, $\phi_{D,2} = 0$

already known (established according to need)

$$\phi_{D,3} = \left(\frac{\phi_{D,1} + \phi_{D,2}}{2L}\right)\left(1 + \frac{L_1}{L}\right)H \quad (11)$$

$$\phi_{D,4} = \phi_{D,6} = \left(\frac{\phi_{D,1} + \phi_{D,2}}{2L}\right)H \quad (12)$$

$$\phi_{D,5} = \left(\frac{\phi_{D,1} + \phi_{D,2}}{2L}\right)\left(1 - \frac{L_2}{L}\right)H \quad (13)$$

These equations allow for the rapid and accurate calculation of the electric potential strengths that should be established in the various channels of the multi-T-form injection system during the loading and dispensing steps in order to mimic the cross-injection model. Table 1 presents the results of these equations for the three fixed configuration injection systems considered in this study for the experiment. Figure 7 shows the electric potential contours and the sample plug distribution for the loading and dispensing steps in the case where the multi-T-form injection system is used to replicate the cross-injection system. With this arrangement, the electric potentials of channels 1−3 and 5 are maintained at a constant value in order to avoid sample plug leakage into channels 1 and 2 and the sample flows from loading channel 6 to waste channel 4 (Figure 8a, loading step). During dispensing, the appropriate electric potential within each channel is established by eqs 11−13 and results in the sample plug being led into the separation channel 2. It is noted from Figure 7 that there is a small leakage of the sample into waste channel 5, but the volume of leakage is negligible and has no impact upon the volume of the sample plug within the separation channel.

Case II: Double-T-Form Injection System Model. In this case, appropriate control of the electric potential within each channel of the multi-T-form injection system allows the injection system to imitate the function of the double-T-form system. The appropriate electric field can be established by the following:

loading step

$\phi_{L,6} = \phi_{max}$, $\phi_{L,4} = \phi_{L,5} = 0$

already known (established according to need)

$$\phi_{L,1} = \phi_{L,3} = \left(\frac{\phi_{L,6} + \phi_{L,4}}{2H}\right)\left(1 + \frac{L_1}{L}\right)L \quad (14)$$

$$\phi_{L,2} = \left(\frac{\phi_{L,6} + \phi_{L,4}}{2H}\right)\left(1 - \frac{L_2}{L}\right)L \quad (15)$$

The electric potentials in the various channels required during the dispensing step in this case are given by eqs 11−13 and are presented in Table 1 (for experiment). The corresponding electric potential contours and sample plug distribution in the loading and

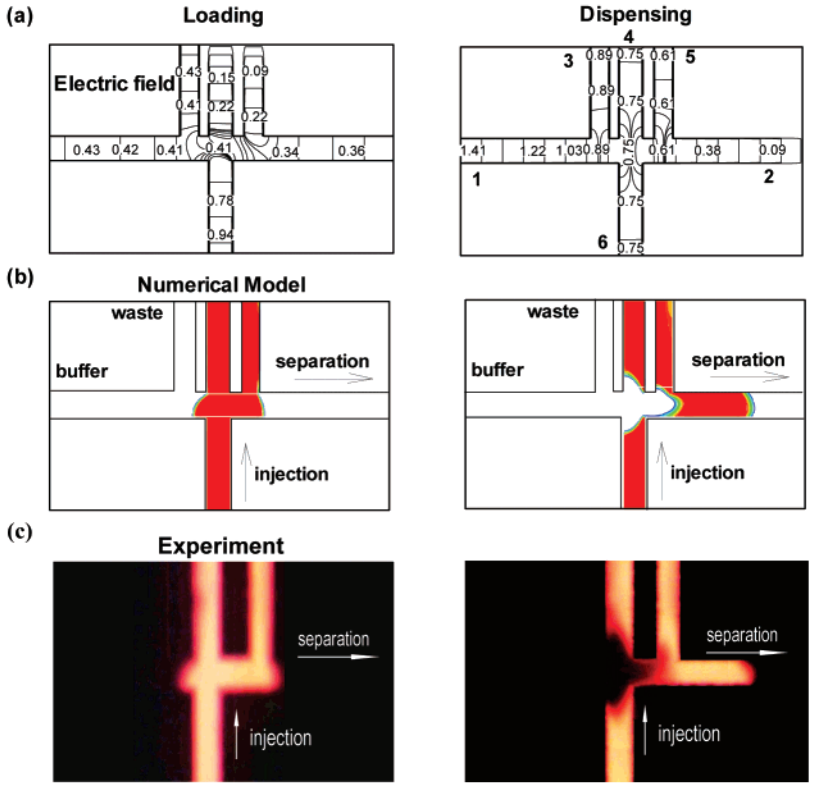

Figure 8. Double-T-form injection model of the multi-T-form injection system.

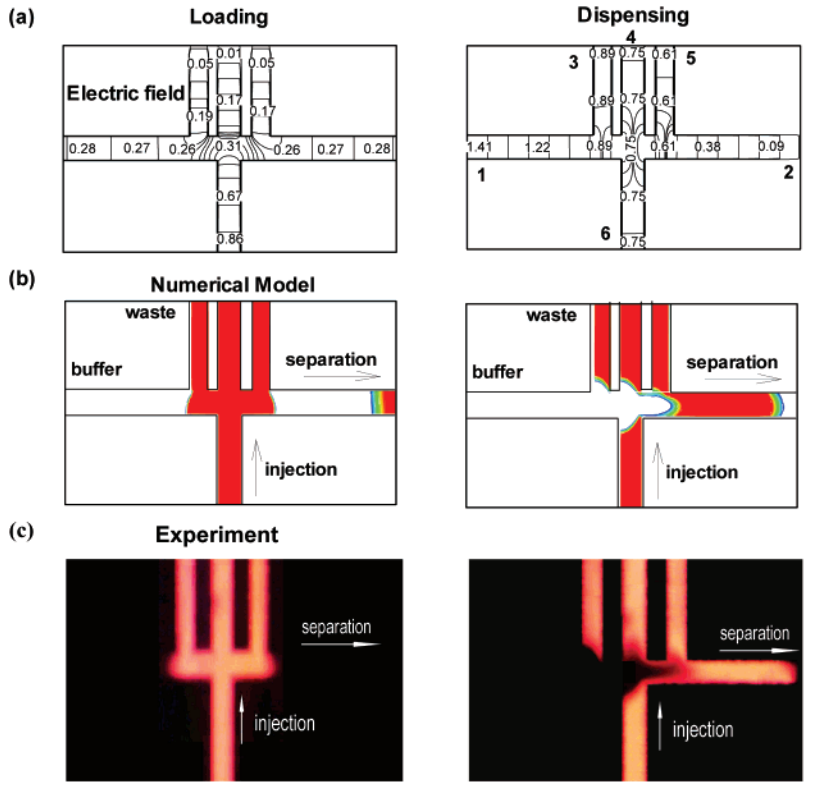

Figure 9. Triple-T-from injection model of the multi-T-form injection system.

dispensing steps are shown in Figure 8. When the appropriate electric potential is applied for the loading step, the sample flows from channel 6 to waste channels 4 and 5. Meanwhile, buffer liquid in the other channels prevents sample leakage (Figure 8a, loading step). The operation of the dispensing step is exactly as described previously for the case where the multi-T-form injection system replicates the cross-injection system. However, it will be observed that the volume of the sample plug in the separation channel is much larger than in the previous case. In other words, the multi-T-form injection system is capable of emulating the double-T-form

injection system.

Case III: Triple-T-Form Injection System Model. In this mode, the electric potentials within the various channels of the multi-T-form injection system are distributed in such a way as to replicate the operation of the triple-T-form injection system, i.e., with the aim of delivering a large-volume sample plug into the separation channel. The appropriate electric potential can be evaluated by means of the following formulas:

loading step

$\phi_{L,6} = \phi_{max}$, $\phi_{L,3} = \phi_{L,4} = \phi_{L,5} = 0$

already known (established according to need)

$$\phi_{L,1} = \left(\frac{\phi_{L,6} + \phi_{L,3}}{2H}\right) \times \left(1 - \frac{L_1}{L}\right)L \quad (16)$$

$$\phi_{L,2} = \left(\frac{\phi_{L,6} + \phi_{L,5}}{2H}\right) \times \left(1 - \frac{L_2}{L}\right)L \quad (17)$$

Table 1 presents the appropriate set of electric potentials within the various microchannels during the loading and dispensing steps. During the loading step there is a linear distribution of the electric potential from channel 6 to channels 3−5 (i.e., $\partial\phi/\partial y \neq 0$). Meanwhile, other than in the region of the intersection area, the potential distribution in channels 1 and 2 is maintained at a constant value (i.e., $\partial\phi/\partial x = 0$). Under such conditions, the sample flows from channel 6 to waste channels 3−5 while the buffer liquid in channels 1 and 2 remains motionless and therefore prevents sample leakage (Figure 9a, loading step). During the dispensing step, the potential distribution is identical to that presented previously for cases I and II. Therefore, the electric field distribution shown in Figure 9 is equivalent to that given in Figures 7 and 8. However, it should be noted that the volume of the sample plug is much greater than in the two previous cases. In fact, observation shows the volume of the sample plug delivered into the separation channel in the case of the simulated triple-T form to be ∼3 times that of case I (cross-injection simulation) and roughly 1.5 times that of the plug delivered in the simulation of the double-T system.

CONCLUSIONS

This paper has presented a physical and numerical study of various injection systems in microfluidic chips. The numerical model provides a useful tool for simulating the process of an injected sample into a separation channel. The formulas presented in this paper confirm that the loading and dispensing steps of an injected sample plug can be successfully controlled through the application of an appropriate set of electric potential distributions. The validity of the proposed numerical approach has been investigated by conducting physical experiments. The results indicate that the distribution of the injected sample plug obtained from the proposed numerical simulation in the cross- and multi-T-form injection system is in good agreement with the experimental results. Furthermore, this study has addressed the design and testing of a unique multi-T-form injection system, which combines the functions of the conventional cross-, double-T-form, and triple-T-form injection systems in a single microfluidic chip. It is the belief of the authors that the results provided in this paper will serve as a valuable reference for the design of injection systems and in the development of the next generation of microfluidic chips.

SUPPORTING INFORMATION AVAILABLE

Additional data as noted in text. This material is available free of charge via the Internet at http://pubs.acs.org.

Received for review June 4, 2002. Revised manuscript received July 24, 2002. Accepted July 31, 2002.

AC025821W